CORE
Metadata, citation and similar papers at core.ac.uk
Provided by Digital.CSIC

Submitted, accepted and published by
Energy Fuels 2014, 28, 7043-7052

On a Highly Reactive Fe_2O_3/Al_2O_3 Oxygen Carrier for *in-situ* Gasification Chemical Looping Combustion (*i*G-CLC)

Daofeng Mei,[†] Alberto Abad,[‡] Haibo Zhao,[*†] Juan Adánez,[‡] Chuguang Zheng[†]

[†]State Key Laboratory of Coal Combustion, Huazhong University of Science and Technology, Wuhan 430074, People's Republic of China

[‡]Department of Energy and Environment, Instituto de Carboquímica (ICB-CSIC), Miguel Luesma Castán 4, Zaragoza 50018, Spain

[*]Corresponding authors. Tel.: +86 27 8754 4779x8208; Fax: +86 27 8754 5526.
E-mail address: klinsmannzhb@163.com (H. Zhao)

Abstract

Interest in the direct use of solid fuel in chemical looping combustion (CLC) technology makes the *in-situ* Gasification Chemical Looping Combustion (*i*G-CLC) an attractive approach for the low-cost capture of CO_2. Highly reactive material is required in *i*G-CLC in order to achieve a fast reaction between the fuel and oxygen carrier. In this work, a material, Fe_2O_3/Al_2O_3 synthesized by sol-gel, was evaluated in a fluidized-bed reactor by reaction with lignite. This is the first time sol-gel-derived Fe_2O_3/Al_2O_3 material has been used in an *i*G-CLC process. Operation conditions, including steam content in the fluidization gas, temperature and potential oxygen ratio were investigated to explore their influence on combustion and char conversion. The results show that a higher steam concentration can greatly enhance the rate of char gasification and hence the reaction between the lignite and the oxygen carrier, whereas a negligible effect of the steam content was noticed on volatile combustion. In addition, the use of the highly reactive Fe-based material prepared by the sol-gel method significantly increased the char gasification rate as compared to other previously evaluated materials. Moreover, the combustion efficiencies of volatiles and char from the lignite, respectively, were studied. Using the Fe_2O_3/Al_2O_3 material enabled a low oxygen carrier inventory of 600 kg/MW_{th} to be reached in order to achieve 99% char combustion, which is much lower than that reported in other works. These findings suggest that Fe_2O_3/Al_2O_3 prepared by sol-gel is a highly reactive oxygen carrier for *i*G-CLC.

Keywords: CO_2 capture, *In-situ* Gasification Chemical-looping Combustion (*i*G-CLC); Sol-gel-derived Fe_2O_3/Al_2O_3 oxygen carrier; Solid fuel; Fluidized-bed reactor

1. Introduction

The concentration of CO_2 as a major contributor to the global warming has greatly increased of its concentration in recent decades. The mean concentration of CO_2 increased to 395 ppm in 2013 [1]. Based on the analyses performed by IPCC and IEA [2, 3], carbon capture and storage (CCS) could attribute something in the range of 15-55% to the cumulative worldwide carbon-mitigation effort until 2100, at a reasonable cost. Based on the rationale of the production of pure CO_2 [4],Chemical Looping Combustion (CLC) is a promising technology for the low-cost capture of CO_2, the purpose for which the CLC concept was first proposed by Richter et al. [5]. CLC technology splits traditional combustion into two separate steps: combustion of fuel through the utilization of the oxygen inherent in metal oxide, and regeneration of the metal oxide. The most common form of CLC operation is that of interconnected reactors, e.g., fluidized-bed combustor [6].

Unlike the conventional CLC process in which gaseous fuel is used, *i*G-CLC utilizes an oxygen carrier to react with the gasification products of solid fuels[7, 8] in order to overcome the low rate of solid-solid reaction between coal and oxygen carrier particles [9-12]. By using the *i*G-CLC process for the combustion of coal, the overall reaction rate can be increased to reasonable levels, while the cost of capturing CO_2 can be greatly reduced. A schematic layout of *i*G-CLC is shown in Figure 1, in which coal and steam [H_2O (g)] are introduced into the fuel reactor where the coal decomposes into volatiles and char via R1. The volatiles react directly with oxygen carrier (here denoted as MeO_x) (R2), while the char is gasified into CO and H_2 by the steam via R3. The gasification products (CO and H_2) subsequently react with the oxygen carrier to produce CO_2 and H_2O via R4 and R5. MeO_x is reduced to MeO_{x-1} in the series of reactions taking place in the fuel

reactor (R1-R5), producing only CO_2 and H_2O at the fuel reactor outlet. Therefore, pure CO_2 can ideally be obtained after removing the steam by condensation at low energy cost. The gasification of the char may be slightly inhibited by the gasification products CO and H_2, which are maintained at low levels due to the presence of the oxygen carrier[13-15]. Even so, the char gasification may be slow enough to allow complete conversion in a one-pass process in the fuel reactor, which results in unconverted char mixing with the oxygen carrier at the fuel reactor outlet. Therefore, the depleted oxygen carrier (MeO_{x-1}) is afterward transferred into the carbon stripper to recover and transfer the unconverted char to the fuel reactor to improve the overall char conversion efficiency and CO_2 capture[9]. The MeO_{x-1} is then transported to the air reactor for regeneration by capturing O_2 from the air via R6, leaving it ready for new cycles. Consequently, *i*G-CLC is a very promising process for the capture of CO_2, with its low energy penalty and low environmental pollution.

Reactions in fuel reactor (R1-R5):

$$\mathrm{Coal} \xrightarrow{\mathrm{HEAT}} \mathrm{Volatiles(CO, H_2, CH_4)} + \mathrm{Char} \quad \text{(R1)}$$

$$\mathrm{Volatiles} + \mathrm{MeO_x} \longrightarrow \mathrm{MeO_{x-1}} + \mathrm{CO_2(g)} + \mathrm{H_2O(g)} \quad \text{(R2)}$$

$$\mathrm{Char} + \mathrm{H_2O(g)} \longrightarrow \mathrm{CO(g)} + \mathrm{H_2(g)} + \mathrm{Ash} \quad \text{(R3)}$$

$$\mathrm{H_2(g)} + \mathrm{MeO_x} \longrightarrow \mathrm{MeO_{x-1}} + \mathrm{H_2O(g)} \quad \text{(R4)}$$

$$\mathrm{CO(g)} + \mathrm{MeO_x} \longrightarrow \mathrm{MeO_{x-1}} + \mathrm{CO_2(g)} \quad \text{(R5)}$$

Reaction in air reactor (R6):

$$\mathrm{Air(g)} + \mathrm{MeO_{x-1}} \longrightarrow \mathrm{MeO_x} + \mathrm{N_2(g)} + \mathrm{O_2(g)} \quad \text{(R6)}$$

The oxygen carrier is the cornerstone of CLC technology. Presently, over 700 oxygen carriers

have been developed for this technology, among which Fe-based materials are highlighted for being low cost and environmental friendly, with low agglomeration or attrition rates and stable reactivity. In this context, some materials, including the synthetic oxygen carriers, natural ore and industrial waste were investigated, with a focus on their reactivity with solid fuels [7]. Natural ore and industrial waste have attracted increasing attention recently due to their low cost. Ilmenite has been identified as a suitable material for use as an oxygen carrier in *i*G-CLC [16] and has been extensively analysed in units ranging from 0.5 to 100 kW [17-19]. Moreover, ilmenite can be activated after a number of cycles with fuel gases [20] or coal [21], which is helpful for decreasing oxygen carrier inventory in CLC systems. The availability and reasonable reactivity of natural iron ores or Fe-derived waste products have been also highlighted for the *i*G-CLC process[12,22,23]. Thus, improved performance was reached in a *i*G-CLC unit with these materials compared to ilmenite [24, 25].

With regard to synthetic materials, Fe_2O_3 is usually supported on inert material in order to improve its active surface and mechanical properties. The mixing between active Fe_2O_3 and the supports is typically conducted by means of chemical or physical synthesis, such as freeze granulation, impregnation, spray drying, co-precipitation, mechanical mixing, etc. $Fe_2O_3/MgAl_2O_4$ material was tested with several coals in a fluidized-bed reactor to demonstrate its availability in *i*G-CLC [16], in which satisfactory reactivity was achieved, similar to that of ilmenite particles.

Coal combustion in the CLC process has been carried out in several experimental units mostly using minerals or waste products as the oxygen carrier [7]. High CO_2 capture rates can be achieved by using a highly effective carbon stripper unit [26]. Other options for increasing char conversion, and hence CO_2 capture, could include increasing the operating temperature and the steam

concentration in the fluidization gas [12, 21]. Furthermore, higher gasification rates can be attained with reactive solids, e.g. lignite or biomass fuel [27, 28]. Nevertheless, unconverted gases (e.g. CO, H_2 and CH_4) were found in all cases where a fluidized bed was used as fuel reactor.[29] The use of highly reactive materials, e.g. red mud or iron ore, has been found to be a good option in terms of improving the reaction rate between oxygen carrier and the gasification products in order to achieve high combustion efficiencies [12, 27].

The use of a highly reactive material as an oxygen carrier was identified as a key factor with which to significantly increase the combustion efficiency of the *i*G-CLC process [30]. Oxygen carrier reactivity would depend on the metal oxide used and the preparation method. For the *i*G-CLC process, iron-based materials based have received great attention because of their low cost and resistance to sulphur [31, 32]. With regard to the structures of oxygen carrier particles developed to date, three types of particles can be involved (see Figure 2). Depending on the synthesis process, oxygen carrier particles can possess (a) a uniform structure with active oxide and support being mixed at a molecular level; (b) a non-uniform distribution of active oxide and support; (c) a uniform structure with active oxide and support distributed separately. Figure 2 shows that, in the case of particle type (b), e.g. impregnated particle, highly reactive materials can be prepared but a high active oxide content is difficult to achieve owing to the limitation of the pore volume of the support; in the case of particle type (c), e.g. prepared by mechanical mixing, freeze granulation or spray drying, a high metal oxide content can be included, but reactivity is lower than that of particles prepared by impregnation. However, these disadvantages can be reasonably avoided in the case of particle (a), which can be produced by means of the sol-gel technique.

Despite the large amount of research carried out on Fe-based oxygen carriers for *i*G-CLC, more studies are necessary for new materials, for instance the sol-gel derived Fe_2O_3/Al_2O_3 in this work. The sol-gel process is usually involved for the preparation of catalyst [33] and sometimes for the oxygen carriers used in CLC technology [34-37]. Particles prepared through the sol-gel technique possess the structure of particle type (a), shown in Figure 2, which has the advantages of controlled size and shape, molecular scale homogeneity, high purity and stoichiometry [33]. Evidently, the sol-gel technique is very different to those used in published works, i.e. freeze granulation, impregnation, spray drying, mechanical mixing, and some characteristics of the sol-gel-derived Fe_2O_3/Al_2O_3 may be different from those of similar materials prepared through other processes. Therefore, it is necessary to evaluate this material in the *i*G-CLC process.

The aim of this work was to evaluate the performance of a sol-gel-derived Fe_2O_3/Al_2O_3 oxygen carrier for coal combustion with CO_2 capture in the *i*G-CLC process. This work is the first time such sol-gel derived materials have been used . The experimental work was carried out in a batch fluidized-bed reactor with coal. The *i*G-CLC process was simulated through successive reduction with lignite and oxidation with pure air in a batch fluidized-bed reactor. Two consecutive steps involved in the combustion of coal with the oxygen carrier were studied: the release and combustion of volatiles, and char gasification and combustion. Special attention was paid to the steam content in the fluidization gas, as regards its effects on volatile combustion, char gasification and oxygen carrier conversion. The influence of reaction temperature on the combustion efficiencies for volatiles and char was studied. The after-use particles of Fe_2O_3/Al_2O_3

were characterized with respect to their physical properties. The potential oxygen ratio between the oxygen carrier and coal, which is related to the solids inventory per thermal MW of fuel, was considered to a factor influencing the combustion process. Oxygen carrier inventories for the combustion of volatiles and char, respectively, were investigated.

2. Experimental

2.1 *Particle materials*

The sol-gel-derived Fe_2O_3 /Al_2O_3 particles were tested for the first time as an oxygen carrier with solid fuels in fluidized-bed reaction system. The sol-gel process had been previously described by Zhao et al. [38] and Mei et al. [35] for the preparation of Ni- and Cu-based oxygen carrier materials. Based on the previous research [39],the present work used 60 wt% Fe_2O_3 as the active oxide supported on Al_2O_3 in order to provide stable conversion and good reactivity . With regard to the preparation of the Fe_2O_3/Al_2O_3 material containing 60 wt% Fe_2O_3, stoichiometric ferric nitrate [$Fe(NO_3)_3 \cdot 9H_2O$, Sinopharm Co., 99.9% purity] and aluminium isopropoxide [$Al(C_3H_7O)_3$, KESHI Co., 99.9% purity] were used, respectively, as precursors. The sol, mainly containing γ-AlOOH, was produced firstly by hydrolysis and ageing of the aluminium isopropoxide for 12 h, where deionized water was used as the hydrolytic agent and 1 mol/L nitric acid was added up to the ratio H^+/Al^{3+}=0.07 to enhance the hydrolysis of aluminium isopropoxide. The gel was obtained by dispersing the stoichiometric amount of ferric nitrate into the sol with a thorough stirring. After drying the wet gel in a step-by-step manner, the dried gel was obtained. This was then subjected to calcination in a muffle furnace at 500^{o}C for 6 h and then at 1200^{o}C for 12 h in air atmosphere. The calcination steps were used to oxidize the Fe and Al elements to Fe_2O_3 and Al_2O_3, as well as to increase the physical strength of products. The conglomerate obtained after calcination was

ground to small particles, which were then sieved to the diameter of 0.125-0.18 mm as the final products. The main characteristics of the Fe_2O_3/Al_2O_3 particles are shown in Table 1. X-ray diffractometer (XRD-7000, SHIMDZU Co.) tests showed that the calcined material was composed of Fe_2O_3 and Al_2O_3, and no impurities were detected. The crushing strength of the particles was 1.39 N, as measured by FGJ-5 (Shimpo Co.), which was the mean force required to fracture the 20 randomly selected particles. According to the statement by Johansson et al. [40], the crushing strength was sufficient for the cycle tests in a fluidized-bed system. The BET surface area of the oxygen carrier particles was 1.39 m^2/g, as measured by N_2 adsorption method (ASAP2020, Micromeritics Co.). The real density of the oxygen carrier was 4653 kg/m^3, which was determined by a density analyser (AccuPyc 1330, Micromeritics Co.). The microstructure of the fresh and used material was examined by an ESEM device (Quanta 200, FEI Co.). Oxygen transport capacity is defined as the ideal fraction of oxygen available in the total mass of oxygen carrier, which is calculated by $R_{OC}=(m_{ox}-m_{red})/m_{ox}$, where m_{ox} and m_{red} denote the mass of oxygen carrier in complete oxidation form and in fully reduced form, respectively. In this work, the oxidized and the reduced forms of the oxygen carrier were determined as Fe_2O_3/Al_2O_3 and Fe_3O_4/Al_2O_3, respectively, see Table 1. Accordingly, the R_{OC} for 60wt% Fe_2O_3 supported on Al_2O_3 was 2.0 %.

The solid fuel employed in this work was a type of lignite from Xiao Longtan, China. The lignite was first dried in an oven for 12 h at 105^oC , and then ground and sieved to 0.18-0.30 mm. This diameter was larger than that of the oxygen carrier, which was helpful for the mixing of oxygen carrier particles and fuel particles, considering the difference in their densities. A proximate and ultimate analysis and the lower heating value (*LHV*) of the lignite are presented in Table 2.

2.2 *Batch fluidized-bed system*

The experimental tests for the *i*G-CLC were carried out in a batch fluidized-bed reactor with lignite as solid fuel. An overview of the fluidized-bed system is presented in Figure 3. A detailed description of this system can be found elsewhere [35, 41]. The steam used in the tests was generated in a heating sleeve located downstream of the water pump. The temperature of the sleeve was controlled at around 250^{o}C to prevent condensation of steam downstream, despite all the pipes connected to the reaction tube being heated. The steam flow rate was controlled by the flow of water through the pump. Steam and pure N_2, fluidization gases were mixed with different steam contents (20-80 vol%) and fed into the reactor at 800 mL/min. The operation conditions for the tests are summarized in Table 3. The reactor temperature was kept stable at between 900ºC and 1000^{o}C by an electric furnace surrounding the tube. Initially, 15 g of oxygen carrier particles were fed into the reactor through the hopper located on the top of the tube and fluidized by pure air at 900^{o}C for 30 min to assure thorough oxidation. 0.1-0.2 g lignite particles were inserted into the hopper in stable conditions, and then pushed into the reactor by pressurized nitrogen gas. Regeneration of the oxygen carrier was conducted by air at a flow rate of 800 mL/min at the same temperature as the reduction. A filter located upstream of the condenser was used to separate the fine particles from the reaction products. Gas products from the reduction and oxidation were first removed from steam in a cooler and subsequently led to a gas analyser (Gasboard 3100) to measure the concentration of CO_2, CO, CH_4, H_2 and O_2. Concentration values were instantaneously recorded by a data logger connected to the computer.

3. Data evaluation

In the *i*G-CLC process, coal fed initially devolatilizes to produce volatiles and char via R1. The volatiles mainly containing CO, H_2 and CH_4 then react with oxygen carriers via R2, whereas char is first gasified to CO and H_2 via R3, subsequently reacting with oxygen carrier particles through R4 and R5. As seen, two consecutive steps are involved in the coal combustion process: volatile evolution and char gasification. As a result, in order to provide a better understanding of the two steps, the evolution of coal, volatile and char conversion with time was calculated in this work.

To analyse the experimental results from the fluidized bed, mass balances to carbon, hydrogen and oxygen were calculated from the concentrations of CO_2, CO, CH_4, H_2 and O_2 in the tests. The rate of carbon conversion, $r_C(t)$ was calculated as eq. 1 where y_i denotes the molar concentration of gas i (CO_2, CO and CH_4) in the dry outlet stream with the flow rate F_{out}.

$$r_C(t) = (y_{CO_2} + y_{CO} + y_{CH_4})F_{out} \qquad \text{(eq. 1)}$$

The conversions of the coal (i=coal) and char (i=char), X_i, were obtained by comparing the carbon produced to that contained in the lignite ($N_{C,coal}$) and in the corresponding char ($N_{C,char}$), which were calculated as eq. 2a and b. The time t_1 in eq. 2b corresponds to the end of coal devolatilization and the beginning of the char gasification.

$$X_{coal} = \frac{\int_0^t r_C(t)dt}{N_{C,coal}} \qquad \text{(eq. 2a)}$$

$$X_{char} = \frac{\int_{t_1}^t r_C(t)dt}{N_{C,char}} \quad (t > t_1) \text{ (eq. 2b)}$$

The instantaneous conversion rates of volatiles (i=volat) and char (i=char), $r_{i,\mathrm{inst}}(t)$, were calculated, respectively, by eq. 3a and b.

$$r_{\mathrm{volat,inst}}(t) = \frac{r_{\mathrm{C}}(t)}{N_{\mathrm{C,volat}} - \int_0^t r_{\mathrm{C}}(t)dt} \quad (t < t_1) \qquad \text{(eq. 3a)}$$

$$r_{\mathrm{char,inst}}(t) = \frac{r_{\mathrm{C}}(t)}{N_{\mathrm{C,char}} - \int_{t_1}^t r_{\mathrm{C}}(t)dt} \quad (t > t_1) \quad \text{(eq. 3b)}$$

In the reduction step, the rate of oxygen transferred from the oxygen carrier to the volatiles and char was denoted as $r_{\mathrm{O},i,\mathrm{red}}(t)$ where i=volat and char for volatiles and char, respectively. The calculation method for $r_{\mathrm{O},i,\mathrm{red}}(t)$ is given in eq. 4.

$$r_{\mathrm{O},i,\mathrm{red}}(t) = 2F_{\mathrm{CO_2}} + F_{\mathrm{CO}} + F_{\mathrm{H_2O}} - F_{\mathrm{H_2O,fed}} - F_{\mathrm{O},i} \qquad \text{(eq. 4)}$$

where $F_{\mathrm{H2O,fed}}$ represents the molar flow of water fed to the experiments and $F_{\mathrm{O},i}$ refers to the inherent oxygen in volatiles (i=volat) and char (i=char), respectively. The outlet flow of water F_{H2O} was calculated by means of the hydrogen balance. The oxygen and hydrogen in coal, see Table 2, were assumed to be reserved only in the volatiles, and thus $F_{\mathrm{O,char}}$=0 and $F_{\mathrm{H,char}}$=0 for the char. The flow rate $F_{\mathrm{O,volat}}$, was calculated by assuming the oxygen to be proportional to the carbon in the volatiles, where $f_{\mathrm{O/C,volat}}$=0.89 for the volatiles from the lignite.

The conversion of oxygen transferred from the oxygen carrier reduction, $X_{\mathrm{O,red}}$, was calculated through the quotient between the oxygen used for coal combustion and the potential amount of oxygen in the oxygen carrier.

$$X_{\mathrm{O,red}} = \frac{1}{N_{\mathrm{O,OC}}} \int_0^t r_{\mathrm{O},i,\mathrm{red}}(t)dt \qquad \text{(eq. 5)}$$

The evolution of oxygen carrier conversion with time for the reduction of the oxygen carrier was

calculated as $X_{OC} = 1\text{-}X_{O,red}$.

For regeneration in air, the rate of oxygen transferred, $r_{O,ox}(t)$, was calculated by the molar-flow difference of O_2 between air and the outlet stream. Thus,, the conversion of oxygen transferred, $X_{O,ox}$, and the X_{OC} for the oxidation were calculated as eq. 6 and eq. 7, respectively.

$$X_{O,ox} = \frac{1}{N_{O,OC}} \int_0^t r_{O,ox}(t)dt \qquad \text{(eq. 6)}$$

$$X_{OC} = X_{OC,red} + X_{O,ox} \qquad \text{(eq. 7)}$$

In eq. 7, $X_{OC,red}$ denotes the final value of X_{OC} after the reduction step.

The potential oxygen ratio, δ, is defined as the oxygen mass potentially stored in oxygen carrier per that needed for the complete combustion of coal, which is related to the solid inventory per thermal MW of fuel and representative for the batch experiments.

$$\delta = \frac{m_{OC} \cdot R_{OC}}{m_{coal} \cdot \Omega_{coal}} \qquad \text{(eq. 8)}$$

where m_{OC}, m_{coal} are the mass of oxygen carrier and coal, respectively; Ω_{coal} denotes the stoichiometric mass of oxygen to reach complete combustion per kg of coal.

The oxygen inventory parameter, $m_{FR,i}$ (i=volat or char), was calculated by eq. 9, where C_i denotes the mass fraction of the carbon in the volatiles (i=volat) or char (i=char), and $m_{C,i}$ denotes the mass of carbon in the volatiles (i=volat) or char (i=char) [42].

$$m_{FR,i} = \frac{m_{OC}}{\frac{LHV}{C_i} \cdot m_{C,i} \cdot r_{C,i,inst}} \qquad \text{(eq. 9)}$$

Combustion efficiency $\eta_{c,i}$ for volatiles (i=volat) or char (i=char) is defined as the oxygen gained by the fuel for its oxidation divided by the oxygen needed to fully oxidize the fuel.

$$\eta_{c,i} = \frac{r_{O,i,red}(t)}{2r_C(t) + 0.5F_{H,i} - F_{O,i}} \qquad \text{(eq. 10)}$$

4. Results and discussion

Figure 4 describes the progression of a typical reaction, in which gas concentration profiles were obtained after correction with the deconvolution method used in a previous work [43] and taking into account the residence time distribution of the gas in the system [44]. The progression began with the release of CO, CH_4 and H_2 from the volatiles in the coal (see the close-up of gas concentration profiles in Figure 4(b)). Some of the volatiles exited the reactor without having reacted with the oxygen carrier because of the effects of bubbling, which led to low contact efficiency between volatiles and oxygen carrier particles. Following the appearance of CO, the CO_2 was detected. In 3 seconds CO_2 concentration reached peak value, ~40 vol.%, which suggests the dramatic reduction of the sol-gel-derived Fe_2O_3/Al_2O_3 in *i*G-CLC using the lignite. This fast reduction led to a rapid decrease in oxygen carrier conversion and a fast increase in coal conversion. Combustion of the lignite was accomplished in 150 s. The final values for $X_{O,red}$ and X_{coal} were 0.59 and 0.91, respectively, which were attributable to the excessive use of oxygen carrier and remaining fine lignite particles from the reactor. As can be seen in Table 1, only a fraction of Fe_2O_3 in the oxygen carrier was reduced to Fe_3O_4 by the lignite, owing to the excessive use of oxygen carrier. Oxidation was performed after purging with N_2 for ~400 s. It is remarkable that no carbon-containing gases were detected in the oxidation. In the duration of 120 s, the oxygen

carrier was fully recovered by reacting with air at 900^{o}C.

For the same reduction process as shown in Figure 4, the X_{coal} and dX_{coal}/dt is plotted in Figure 5 to identify the volatile evolution and the char gasification steps. As seen, X_{coal} can be identified as three parts: 0< X_{coal} <=0.06, 0.06< X_{coal} <=0.58 and 0.58< X_{coal} <=0.91, which is related to the different reaction processes and agrees well with the content of volatiles from proximate analysis, see Table 2. The behaviour of coal in *i*G-CLC involves the release of volatiles, the reaction between volatiles and oxygen carrier particles, the gasification of char and the simultaneous reaction of gas products with the oxygen carrier. During the part 0< X_{coal} <=0.06, volatiles were released more and more quickly as the coal particles were heated. After contact between the volatiles and the oxygen carrier particles, 0.06< X_{coal} <=0.58, the coal conversion rate decreased, which was attributable to the decrease in the volatile content in the coal during devolatilization. The conversion rate of coal for 0.58< X_{coal} <=0.91 was lower than that of the previous part owing to the slow gasification of char. In this respect, it is evident that char gasification is the most important step in the *i*G-CLC process to achieve a high CO_2 capture rate. Consequently, the combustion of the lignite can be divided into two zones by X_{coal}=0.58, and this is significant for accelerating char gasification .

In a practical system, the steam content varies along the height of the fuel reactor, which might lead to different rates of reactions [26, 30]. Therefore tests were subsequently conducted at 900^{o}C under different steam contents (20-80 vol%) in order to evaluate the effect of steam on the reaction processes. The effects of steam content are gathered in Table 4 for the oxidation of

volatiles and char. The conversion degree of oxygen in the oxygen carrier for the oxidation of volatiles barely changed under various steam contents. A oxygen carrier conversion of 0.21 (not shown in Table 4) was achieved under different steam concentrations varying between 20 and 80 vol%, which indicates that the combustion efficiency of volatiles and gasification products was at the same level for all the cases. With regard to the cases using 20 and 40 vol% steam contents, a similar volatile combustion efficiency was reached, around 0.62. These findings are related with the low contact efficiency between oxygen carrier particles and volatiles in the volatile plume, similar to that observed by Cuadrat et al. [45]. Moreover, a constant rate of volatiles conversion could be observed when 20 or 40 vol% steam was used, and therefore the calculated oxygen carrier inventory in the fuel reactor for the combustion of volatiles was scarcely changed. Consequently, low relevance of volatile combustion with the steam concentration was noticed.

In the case of the conversion for char, Figure 6 shows the instantaneous rates of char conversion $r_{char,inst}(t)$ as a function of char conversion X_{char}. Unlike volatile evolution, char conversion exhibited high relevance with the steam concentration in the reactor. Higher rates of char conversion can be observed in Figure 6 and Table 4, which are attributable to the higher rates of char gasification with higher steam content. It should be noted that a constant rate of char conversion can be reached when using 80 vol% H_2O. Indeed, as shown in Table 4, the char conversion rates can be ranked to 204 %/min in 80 vol% H_2O, which is much higher than those reported by Mendiara et al. using a low-cost haematite as an oxygen carrier [46]. Moreover, the steam contents also show their effects on the conversion of oxygen carrier, as depicted in Figure 7. A rise in the rate of oxygen transferred could be found for higher steam content both in reduction and oxidation, which was related to the faster char conversion and the higher evolution rate of

gasification products. As a consequence, a lower oxygen carrier inventory was calculated in the case of higher steam concentrations for the gasification of char, see Table 4. It is important to observe that the oxygen carrier was able to be totally recovered in the oxidation in Figure 7 for all the cases.

Operating temperature determines the reaction kinetics between oxygen carrier and fuels. However, the amount of oxygen carrier and fuel influences the efficiency of combustion. Therefore, this section focuses on the influence of operating temperature and potential oxygen ratio (δ) on combustion performance. It is worth noting that the char gasification rate was enhanced by the decrease in the H_2 content of reacting gases in the presence of the oxygen carrier. This fact has been observed in previous works [15, 46, 47]. Reactivity does not have a direct effect on the char gasification rate, as the solid-solid reaction between oxygen carrier and carbon in char particles has little influence on char gasification in a fluidized bed reactor [48]. Hence, the effect was due to the actual H_2 concentration in the reacting atmosphere, as described above. Thus, as gasification products were completely converted to CO_2 and H_2O, gasification was the only step limiting the process, which meant that the evaluation of oxygen carrier reactivity could not be properly conducted. In order to evaluate the effect of oxygen carrier reactivity on the char conversion, experimental conditions must be chosen in order to produce incomplete combustion of gasification products.

Table 5 gathers the values of instantaneous conversion of char $r_{char,inst}$, and char combustion efficiency $\eta_{c,char}$, at different variable pairs, i.e. temperature and potential oxygen ratio (δ). When a fixed potential oxygen ratio was used, e.g. δ=1.77, the operation temperature showed a positive

influence on the fast and efficient combustion of char; as seen, the values of $r_{char,inst}$ and $\eta_{c,char}$ were increased at higher temperatures. This was mainly attributable to the faster gasification of char at higher temperatures. For the cases using 0.15 and 0.2 g coals at 1000^{o}C, i.e. δ=1.18 and 0.88, combustion efficiency decreased greatly at lower potential oxygen ratios. To this end, the oxygen carrier should be sufficient for the combustion of the intermediate from char gasification to achieve higher combustion efficiencies with regard to the sol-gel-derived Fe_2O_3/Al_2O_3 material and the lignite fuel.

No agglomeration or defluidization was found for oxygen carrier particles during operations at temperatures higher than 900^{o}C . The BET surface area for the after-use oxygen carrier particles was 1.31 m^2/g, which were barely changed with respect to the fresh particles (see Table 1). Furthermore, the morphology analysis, as shown in Figure 8, offers proof for this statement. Some larger grains seem to emerge in the after-use particles, albeit no obvious change in microstructure were found in the ESEM pictures. Sintering was avoided in the multiple tests with lignite for *i*G-CLC, since a porous structure was kept.

As mentioned, the sol-gel-derived Fe_2O_3/Al_2O_3 oxygen carrier exhibited higher reactivity than the low-cost haematite studied by Mendiara et al. [46]. It is also significant to compare its reactivity with respect to other synthetic Fe_2O_3/Al_2O_3 materials. The Fe_2O_3/Al_2O_3 oxygen carriers prepared by mechanical mixing and impregnation, which were recently reported by Guo et al. [49], are included for the purpose of comparison. The same reactor, lignite and reaction conditions used in the present work and the previous work [49] eliminate the influence of operating conditions. It can be observed from Figure 9(a) that the sol-gel derived Fe_2O_3/Al_2O_3 material leads to faster char

gasification than the other materials prepared by mechanical mixing and impregnation. This is a result of the higher combustion efficiency for the sol-gel material (see Figure 9(b)). Thus, the inhibiting effect of H_2 on steam gasification is minimized. In this sense, the sol-gel-derived Fe_2O_3/Al_2O_3 oxygen carrier has higher reactivity than the ones synthesized by mechanical mixing and impregnation, which should improve the CO_2 capture rate and the combustion efficiency of the *i*G-CLC process.

It was considered of interest to compare the presented material with the reported Fe-based ones. The method presented by Abad et al. [42] was used in order to properly compare data obtained with different oxygen carrier to char mass ratio values. Thus, the oxygen carrier to char mass ratio was related to a solids inventory value in the fuel reactor, and combustion efficiency values obtained during the experimental campaign were compared. This part gives an intuitive comparison of oxygen carrier inventory with the results reported by other researchers. As shown in Figure 10, a larger oxygen carrier inventory led to higher combustion efficiency $\eta_{c,char}$, which showed a similar trend to that observed by Abad et al.[42] With regard to the significance of char gasification in the *i*G-CLC process, the oxygen carrier inventory required for the oxidation of char in this work was compared with that in the published works [13, 42, 50] in which ilmenite, a haematite-based mineral, bauxite waste and a synthetic material were used. As shown in Figure 10, an oxygen carrier inventory >1500 kg/MW_{th} was required in order to achieve the complete combustion of char in the published works, despite some materials having high reactivity, e.g. mineral and synthetic Fe_2O_3 materials. In contrast, the combustion of char from the lignite required an extremely low oxygen carrier inventory when the sol-gel-derived Fe_2O_3/Al_2O_3 oxygen carrier was used; the lowest

oxygen carrier inventory to achieve combustion efficiency $\eta_{c,char}$=0.99 was 600 kg/MW_{th}. Consequently, the use of the sol-gel derived Fe_2O_3/Al_2O_3 leads to a lower oxygen carrier inventory in fuel reactor, which is beneficial for lowering costs throughout the *i*G-CLC system.

Conclusions

This work performed the first use of sol-gel-derived Fe_2O_3/Al_2O_3 as an oxygen carrier in the *i*G-CLC process. A type of lignite from China was used as the combustion agent, which exhibited satisfactory performance in the combustion processes involved in this work. Steam content had little influence on the combustion of volatiles, whereas it exhibited important effects on the gasification process of char from the lignite. The increase in steam content led to faster gasification and thus higher reaction rates between the coal and the oxygen carrier. The reduced oxygen carrier was able to be fully recovered with a reasonable reaction rate during subsequent oxidation by pure air at the same temperatures as those of reduction. Char gasification determined the reaction rate in the fuel reactor, and this process could be enhanced by using higher operating temperatures. The combustion efficiency of char was highly dependent on the oxygen carrier inventory; the higher the oxygen carrier inventory, the higher the combustion efficiency. In comparison with the published works, an extremely low oxygen carrier inventory, 600 kg/MW_{th} at 900^{o}C, was required for 99% combustion of char with the sol-gel-derived Fe_2O_3/Al_2O_3. No agglomeration or defluidization was found in any of the experiments, and no change in the porous microstructure was observed. The findings in this work suggest that the sol-gel-derived Fe_2O_3/Al_2O_3 material is a highly reactive oxygen carrier for *i*G-CLC. By using this oxygen carrier,

an extremely low oxygen carrier inventory in the fuel reactor can be achieved.

Acknowledgements

This work was supported by "National Natural Science Foundation of China (51390494)", and "National Basic Research and Development Program (2011CB707300)". Daofeng Mei is grateful for the support provided by the Chinese Scholar Council (CSC201306160054). Appreciation is also shown to the staff of the Analytical and Testing Center, Huazhong University of Science and Technology for the related experimental analysis.

Nomenclature

C_i	Mass fraction of the carbon of volatiles (*i*=volat) or char (*i*=char) in the coal
F_i	Molar flow of gas *i* (CO_2, CO, CH_4, H_2, H_2O, N_2, O_2, air) in the reaction products (mol/s)
$F_{H,char}$	Molar flow of H in char entering into the fuel reactor (mol/s)
$F_{H2O,fed}$	Molar flow of water fed into the reactor (mol/s)
$F_{O,i}$	Molar flow of oxygen in volatiles (*i*=volat) or char (*i*=char) (mol/s)
F_{out}	Molar flow of the outlet gas for reduction (mol/s)
$f_{O/C,volat}$	Oxygen to carbon ratio in the volatiles from coal (-)
LHV	Lower heating value of coal (MJ/kg)
$m_{C,i}$	Mass of carbon in volatiles (*i*=volat) or char (*i*=char)
m_{coal}	Mass of coal (kg)
$m_{FR,i}$	Oxygen carrier inventory for the combustion of volatiles (*i*=volat) and char (*i*=char)

m_{OC}	Mass of oxygen carrier (kg)
m_{ox}	Mass of oxygen carrier in complete oxidation form (Fe_2O_3/Al_2O_3, in this work) (kg)
m_{red}	Mass of oxygen carrier in complete reduction form (Fe_3O_4/Al_2O_3, in this work) (kg)
$N_{C,i}$	Moles of carbon contained in the coal (i=coal), volatiles (i=volat) or char (i=char) (mol)
$N_{O,OC}$	Moles of potential oxygen in the oxygen carrier (mol)
$r_C(t)$	Rate of carbon conversion (mol/s)
$r_{i,inst}(t)$	Instantaneous conversion rate of carbon in volatiles (i=volat) or char (i=char) (%/min)
$r_{O,ox}(t)$	Rate of oxygen transfer in oxidation process (mol/s)
$r_{O,i,red}(t)$	Rate of oxygen transfer in reduction with volatiles (i=volat) or char (i=char) (mol/s)
R_{OC}	Oxygen transport capacity of oxygen carrier (-)
t	Time (s)
t_1	Time for the beginning of char gasification (s)
X_{coal}	Conversion of coal (-)
X_{OC}	Conversion of oxygen carrier in redox (-)
$X_{OC,red}$	Final value of X_{OC} after the reduction step
$X_{O,ox}$	Conversion of oxygen for oxidation (-)
$X_{O,red}$	Conversion of oxygen for reduction (-)
$X_{O,i,f}$	Final conversion of oxygen for reduction (i=red) or oxidation (i=ox) (-)
y_i	Molar concentration of gas i (CO_2, CO, CH_4, H_2, H_2O, N_2, O_2) in the products (-)
δ	Potential oxygen ratio, defined as the potential oxygen stored in oxygen carrier per

that required for the complete combustion of fuel (-)

$\eta_{c,i}$ Combustion efficiency for volatiles (i=volat) or char (i=char) (-)

Ω_{coal} Stoichiometric mass of oxygen to convert per kg of coal (-)

References

(1) NOAA-ESRL. *Average Concentration of CO_2 in the Atmosphere (Mauna Loa Observatory) for 2013 was Posted June 14*. 2014. <http://www.esrl.noaa.gov/gmd/ccgg/trends/global.html>

(2) IEA. *Energy Technology Perspectives 2010*. in: *Scenarios and Strategies to 2050*; OECD/IEA: Paris, 2010.

(3) Metz, B.; Davidson, O.; de Coninck, H.; Loos, M.; Meyer, L. *Carbon dioxide capture and storage*; Cambridge University Press: UK, 2005.

(4) Lewis, W. K.; Gilliland, E. R. *Production of pure carbon deoxide*; U.S. Patent 2,665,972, 1954.

(5) Richter H. J.; Knoche K. F. *Reversibility of Combustion Processes*. in: *Efficiency and Costing*; American Chemical Society: Washington, DC, 1983.

(6) Lyngfelt, A.; Leckner, B.; Mattisson, T. *Chem. Eng. Sci.* **2001,** 56, 3101-3113.

(7) Adánez, J.; Abad, A.; García-Labiano, F.; Gayán, P.; de Diego, L. F. *Prog. Energy Combust. Sci.* **2012,** 38, 215-282.

(8) Dennis, J. S.; Scott, S. A.; Hayhurst, A. N. *J. Energy Inst.* **2006,** 79, 187-190.

(9) Cao, Y.; Pan, W. P. *Energy Fuels* **2006,** 20, 1836-1844.

(10) Wang, B.; Yan, R.; Zheng, Y.; Zhao, H.; Zheng, C. *Fuel* **2011,** 90, 2359-2366.

(11) Fan, L. S. *Chemical looping systems for fossil energy conversions*; John Wiley & Sons, 2011.

(12) Mendiara, T.; García-Labiano, F.; Gayán, P.; Abad, A.; de Diego, L. F.; Adánez, J. *Fuel* **2013,**

814-826.

(13) Leion, H.; Mattisson, T.; Lyngfelt, A. *Fuel* **2007,** 86, 1947-1958.

(14) Keller, M.; Leion, H.; Mattisson, T.; Lyngfelt, A. *Combust. Flame* **2011,** 158, 393-400.

(15) Cuadrat, A.; Abad, A.; de Diego, L. F.; García-Labiano, F.; Gayán, P.; Adánez, J. *Fuel* **2012,** 97, 219-232.

(16) Leion, H.; Mattisson, T.; Lyngfelt, A. *Int. J. Greenhouse Gas Control* **2008,** 2, 180-193.

(17) Cuadrat, A.; Abad, A.; García-Labiano, F.; Gayán, P.; de Diego, L. F.; Adánez, J. *Energy Procedia* **2011,** 4, 362-369.

(18) Berguerand, N.; Lyngfelt, A. *Fuel* **2008,** 87, 2713-2726

(19) Markström, P.; Linderholm, C.; Lyngfelt, A. In *proceeding of the 2nd International Conference on Chemical Looping*, Darmstadt, Germany, 2012.

(20) Adánez, J.; Cuadrat, A.; Abad, A.; Gayán, P.; de Diego, L. F.; García-Labiano, F. *Energy Fuels* **2010,** 24, 1402-1413.

(21) Cuadrat, A.; Abad, A.; García-Labiano, F.; Gayán, P.; de Diego, L. F.; Adánez, J. *Int. J. Greenhouse Gas Control* **2011,** 5, 1630-1642.

(22) Song, T.; Shen, T.; Shen, L.; Xiao, J.; Gu, H.; Zhang, S. *Fuel* **2013,** 104, 244-252.

(23) Zhang, S.; Saha, C.; Yang, Y.; Bhattacharya, S.; Xiao, R. *Energy Fuels* **2011,** 25, 4357-4366.

(24) Mendiara, T.; de Diego, L. F.; García-Labiano, F.; Gayán, P.; Abad, A.; Adánez, J. *Int. J. Greenhouse Gas Control* **2013,** 17, 170-182.

(25) Mendiara, T.; de Diego, L. F.; García-Labiano, F.; Gayán, P.; Abad, A.; Adánez, J. *Fuel* **2014,** 126, 239-249.

(26) Abad, A.; Adánez, J.; de Diego, L. F.; Gayán, P.; García-Labiano, F.; Lyngfelt, A. *Int. J.*

Greenhouse Gas Control **2013,** 19, 541-551.

(27) Mendiara, T.; Abad, A.; de Diego, L. F.; García-Labiano, F.; Gayán, P.; Adánez, J. *Int. J. Greenhouse Gas Control* **2013,** 19, 322-330.

(28) Gu, H.; Shen, L.; Xiao, J.; Zhang, S.; Song, T. *Energy Fuels* **2011,** 25, 446-455.

(29) Gayán, P.; Abad, A.; de Diego, L. F.; García-Labiano, F.; Adánez, J. *Chem. Eng. J.* **2013,** 233, 56-69.

(30) García-Labiano, F.; Diego, L. F. d.; Gayán, P.; Abad, A.; Adánez, J. *Chem. Eng. Sci.* **2013,** 87, 173-182.

(31) Cabello, A.; Dueso, C.; García-Labiano, F.; Gayán, P.; Abad, A.; de Diego, L. F.; Adánez, J. *Fuel* **2014,** 121, 117-125.

(32) de Diego, L. F.; García-Labiano, F.; Gayán, P.; Abad, A.; Cabello, A.; Adánez, J.; Sprachmann, G.. *Int. J. Greenhouse Gas Control* **2014,** 28, 168-179.

(33) Brinker, C. J.; Scherer, G. W. *Sol-gel science: the physics and chemistry of sol-gel processing*; Gulf Professional Publishing, 1990.

(34) Ishida, M.; Jin, H.; Okamoto, T. *Energy Fuels* **1996,** 10, 958-963.

(35) Zhao, H.; Liu, L.; Wang, B.; Xu, D.; Jiang, L.; Zheng, C.. *Energy Fuels* **2008,** 22, 898-905.

(36) Mei, D.; Zhao, H.; Ma, Z.; Zheng, C. *Energy Fuels* **2013**, 27, 2723-2731.

(37) Kierzkowska, A. M.; Bohn, C. D.; Scott, S. A.; Cleeton, J. P.; Dennis, J. S.; Müller, C. R. *Ind. Eng. Chem. Res.* **2010,** 49, 5383-5391.

(38) Zhao, H.; Liu, L.; Xu, D.; Zheng, C.; Liu, G.; Jiang, L. *J. Fuel Chem. Technol.* **2008,** 36, 261-266.

(39) Zhao, H.; Mei, D.; Ma, J.; Zheng, C. *Asia-Pacific J. Chem. Eng.* **2014**, DOI: 10.1002/apj.1791.

(40) Johansson, M.; Mattisson, T.; Lyngfelt, A. *Ind. Eng. Chem. Res.* **2004,** 43, 6978-6987.

(41) Zhao, H.; Wang, K.; Fang, Y.; Ma, J.; Mei, D.; Zheng, C. *Int. J. Greenhouse Gas Control* **2014,** 22, 154-164.

(42) Abad, A.; Cuadrat, A.; Mendiara, T.; García-Labiano, F.; Gayán, P.; de Diego, L. F.; Adánez, J. *Ind. Eng. Chem. Res.* **2012,** 51, 16230-16241.

(43) Abad, A.; Mattisson, T.; Lyngfelt, A.; Johansson, M. *Fuel* **2007,** 86, 1021-1035.

(44) Levenspiel, O. *Chemical reaction engineering*; New York etc.: Wiley. 1972.

(45) Cuadrat, A.; Abad, A.; García-Labiano, F.; Gayán, P.; de Diego, L. F.; Adánez, J. *Chem. Eng. J.* **2012,** 195-196, 91-102.

(46) Mendiara, T.; Pérez, R.; Abad, A.; de Diego, L. F.; García-Labiano, F.; Gayán, P.; Adánez, J. *Ind. Eng. Chem. Res.* **2012,** 51, 16216-16229.

(47) Mendiara, T.; Gayán, P.; Abad, A.; de Diego, L. F.; García-Labiano, F.; Adánez, J. *Fuel Process. Technol.* **2013,** 109, 57-69.

(48) Mendiara, T.; García-Labiano, F.; Gayán, P.; Abad, A.; de Diego, L. F.; Adánez, J. *Fuel* **2013,** 106, 814-826.

(49) Guo, L.; Zhao, H.; Ma, J.; Mei, D.; Zheng, C. *Chem. Eng. Technol.* **2014,** 37, 1211-1219.

(50) Jerndal, E.; Leion, H.; Axelsson, L.; Ekvall, T.; Hedberg, M.; Johansson, K.; Källén, M.; Svensson, R.; Mattisson, T.; Lyngfelt, A. *Oil Gas Sci. Technol.–Revue d'IFP Energies nouvelles* **2011,** 66, 235-248.

Figure Captions

Figure 1 Schematic layout of *i*G-CLC process

Figure 2 Three types of structure for the oxygen carrier particles developed through different techniques

Figure 3 An overview of the fluidized-bed reactor

Figure 4 (a) Profiles of gas concentration, conversion of oxygen carrier (X_{OC}) and conversion of coal (X_{coal}) in a typical reduction-oxidation cycle at 900^{o}C; (b) Close-up of the gas concentration profiles for the first 100 seconds, t=t_1 shows the beginning of char gasification; 0.1 g lignite and 40 vol % H_2O were used

Figure 5 dX_{coal}/dt changes as a function of X_{coal} at 900 ^{o}C; 0.1 g lignite and 40 vol% H_2O were used

Figure 6 Instantaneous rate of char conversion, $r_{char,inst}(t)$, as a function of the char conversion during the gasification period at 900^{o}C; fluidization gases with 20-80 vol% steam were used; 0.1 g lignite was used

Figure 7 Final conversion of oxygen transferred in reduction and oxidation processes as a function of steam content; tests were carried out at 900^{o}C fluidized with 20-80 vol% steam; 0.1 g lignite was used

Figure 8 Morphology analysis of the fresh oxygen carrier particles (left) and the after-use particles (right), in the vision of 10000x, the bar corresponds to the length of 5 μm

Figure 9 Comparison of char gasification rate, $r_{char,inst}$, and char combustion efficiency, η_{char}, for the combustion of lignite with different Fe_2O_3/Al_2O_3 oxygen carriers prepared by sol-gel (SG), Mechanical mixing (MM) and impregnation (IMP); Condition: 0.1g lignite, 80 vol% H_2O, 1000^{o}C

Figure 10 Char combustion efficiency, $\eta_{c,char}$, as a function of the oxygen carrier inventory in fuel reactor, $m_{FR,char}$, compared with the published values for different oxygen carriers and coal chars collected from published works [13, 42, 50]; the temperature is 900^{o}C

Figure 1 Schematic layout of *i*G-CLC process

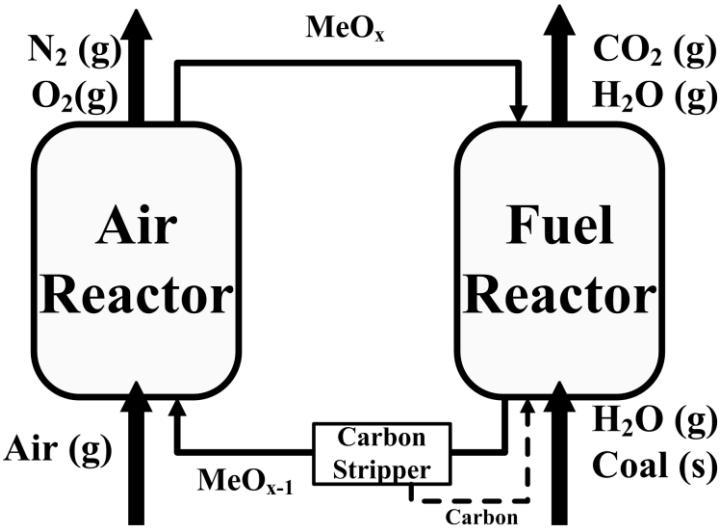

Figure 2 Three types of structure for the oxygen carrier particles developed through different techniques

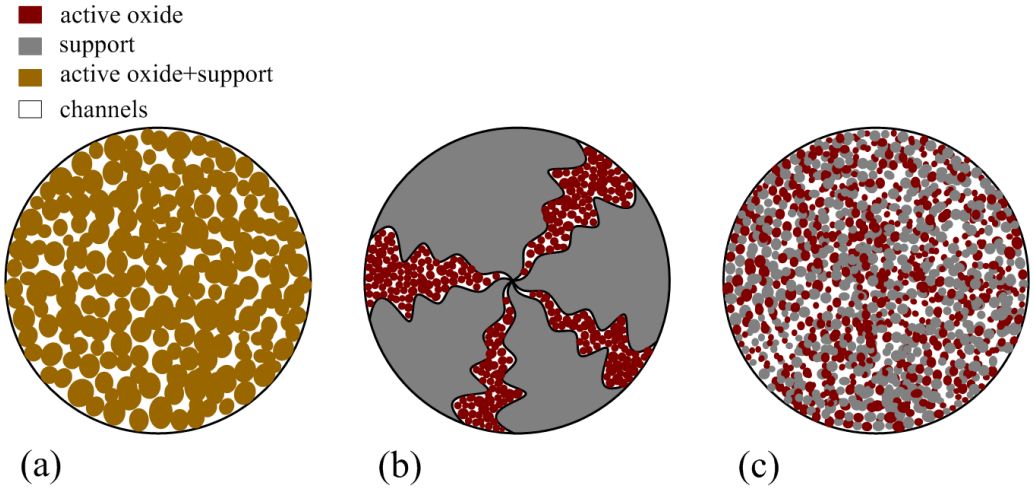

Figure 3 An overview of the fluidized-bed reactor

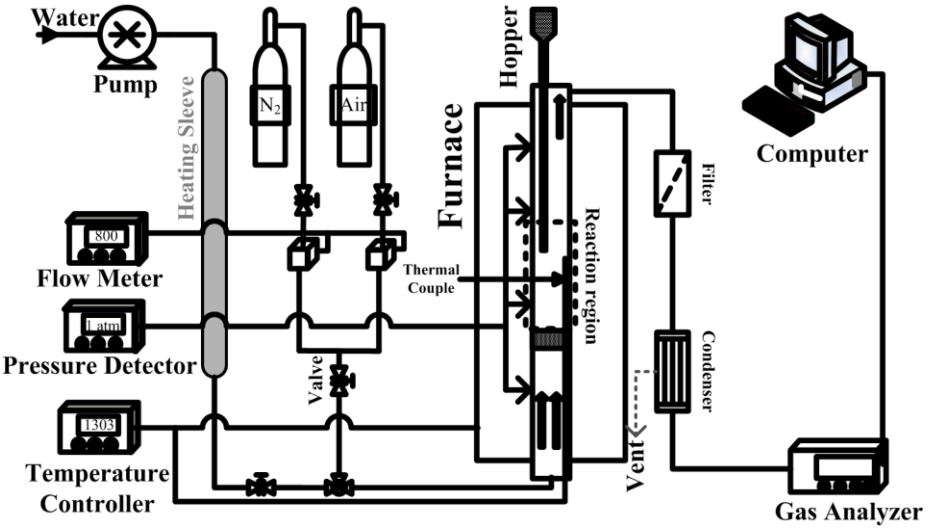

Figure 4 (a) Profiles of gas concentration, conversion of oxygen carrier (X_{OC}) and conversion of coal (X_{coal}) in a typical reduction-oxidation cycle at 900^{o}C; (b) Close-up of the gas concentration profiles for the first 100 seconds, t=t_1 shows the beginning of char gasification; 0.1 g lignite and 40 vol%H_2O were used

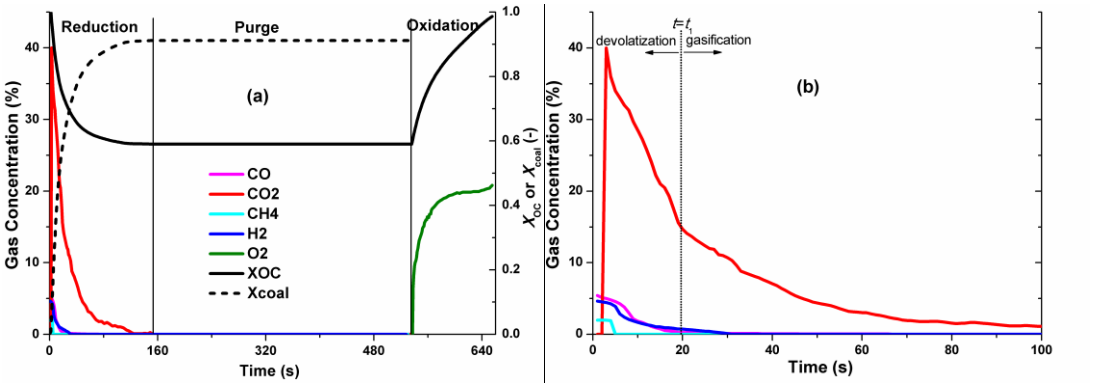

Figure 5 dX_{coal}/dt changes as a function of X_{coal} at 900^{o}C; 0.1 g lignite and 40 vol% H_2O were used

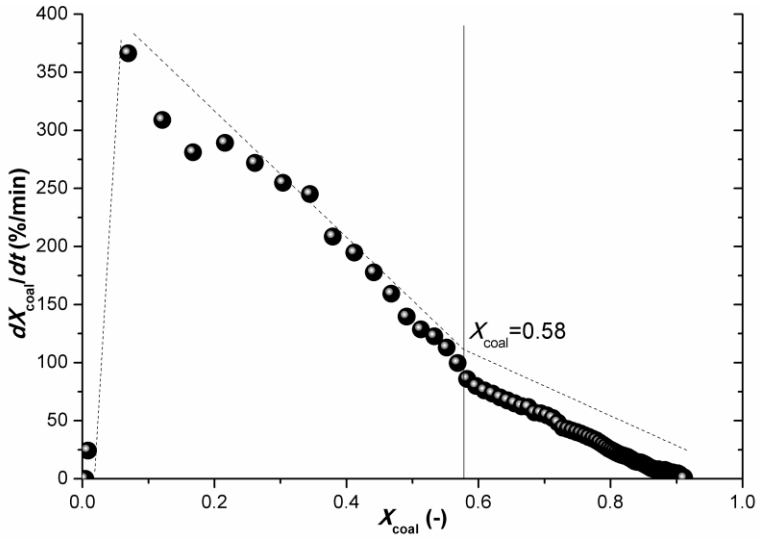

Figure 6 Instantaneous rate of char conversion, $r_{char,inst}(t)$, as a function of the char conversion during the gasification period at 900^{o}C; fluidization gases with 20-80 vol% steam were used; 0.1 g lignite was used

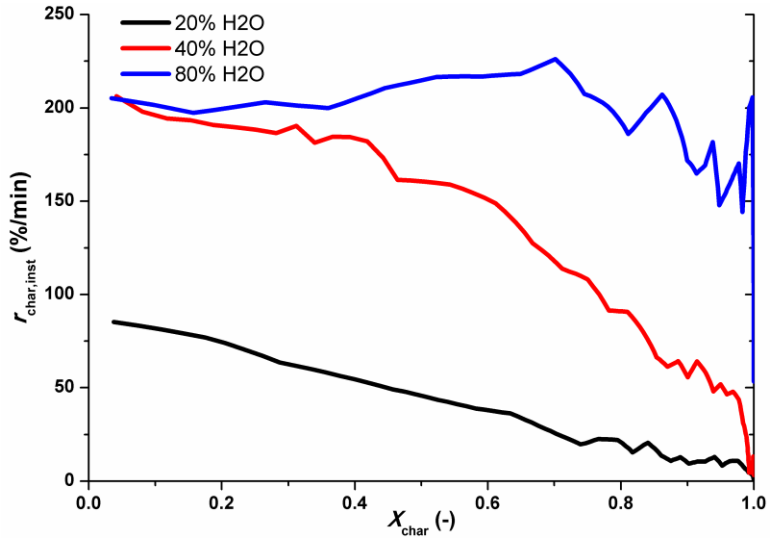

Figure 7 Final conversion of oxygen transferred in reduction and oxidation processes as a function of steam content; tests were carried out at 900^{o}C fluidized with 20-80 vol% steam; 0.1 g lignite was used

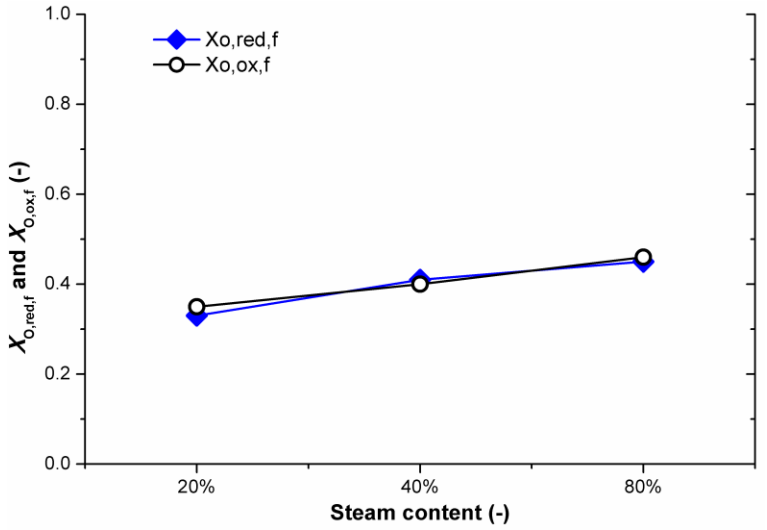

Figure 8 Morphology analysis of the fresh oxygen carrier particles (left) and the after-use particles (right), in the vision of 10000x, the bar corresponds to a length of 5 μm

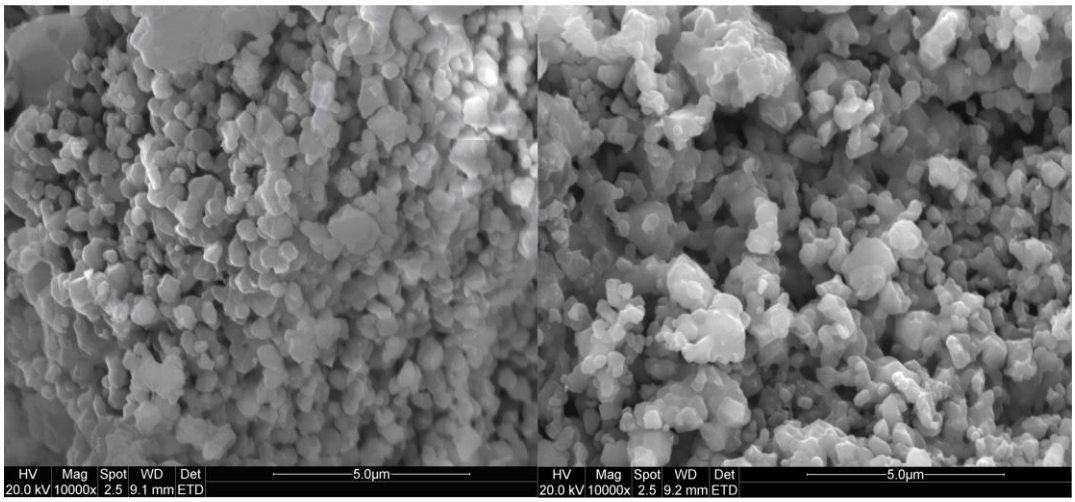

Figure 9 Comparison of char gasification rate, $r_{char,inst}$, and char combustion efficiency, η_{char}, for the combustion of lignite with different Fe_2O_3/Al_2O_3 oxygen carriers prepared by sol-gel (SG), Mechanical mixing (MM) and impregnation (IMP); Condition: 0.1g lignite, 80 vol% H_2O, 1000 ^oC

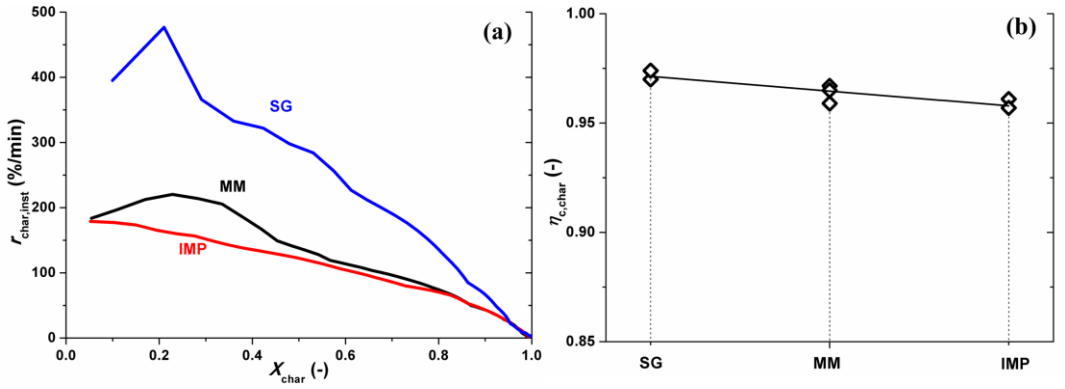

Figure 10 Char combustion efficiency, $\eta_{c,char}$, as a function of the oxygen carrier inventory in fuel reactor, $m_{FR,char}$, compared with the published values for different oxygen carriers and coal chars collected from published works [13, 42, 50]; the temperature is 900^{o}C

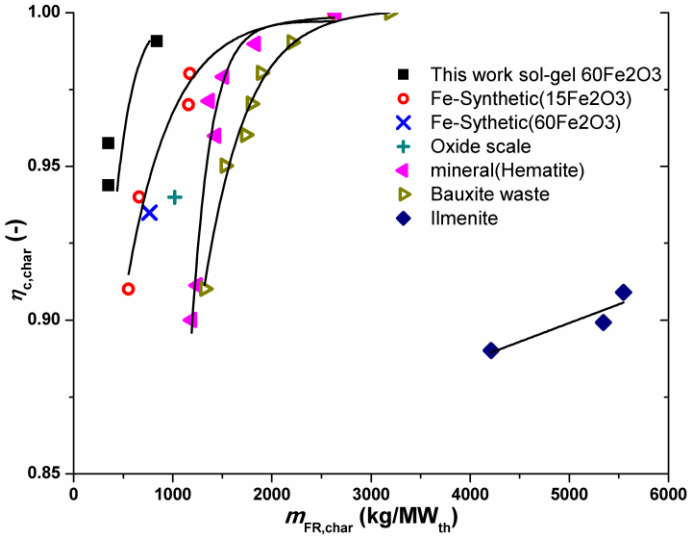

Table Captions

Table 1 Main characteristics of the sol-gel derived Fe_2O_3/Al_2O_3

Table 2 A proximate and ultimate analysis of the lignite

Table 3 Main operating data for the fluidized-bed tests

Table 4 Effect of steam content on the reaction performance, 900^oC, δ=1.77

Table 5 Effects of oxygen potential oxygen ratio δ and temperature on the char combustion, steam content 80 vol%

Table 1 Main characteristics of the sol-gel-derived Fe_2O_3/Al_2O_3

XRD phases	Oxidized: Fe_2O_3, Al_2O_3 Reduced: Fe_3O_4, Fe_2O_3, Al_2O_3
Weight fraction of Fe_2O_3 (wt%)	60
Particle size (mm)	0.125-0.180
Real density (kg/m^3)	4653
Mechanical strength (N)	1.39
BET surface area (m^2/g)	1.39
Oxygen capacity, R_{OC} (%)	2.0

Table 2 A proximate and ultimate analysis of the lignite

Proximate analysis (wt%, dry basis)				Ultimate analysis (wt%, dry basis)					
Moisture	Volatiles	Ash	Fix carbon	C	H	N	S	O[a]	*LHV*[b] (MJ/kg)
4.56	47.08	8.64	39.21	57.42	4.57	1.70	1.47	21.64	20.47

[a] Oxygen to balance, [b] Lower heating value

Table 3 Main operating data for the fluidized-bed tests

Parameter	Description
Oxygen carrier	60 wt% Fe_2O_3/Al_2O_3
Operating temperature	900-1000^oC
Mass of oxygen carrier (g, m_{OC})	15
Solid fuel	Xiao Longtan lignite
Mass of the fuel (g, m_{coal})	0.1-0.2
Potential oxygen ratio (δ)	0.88-1.77
Gasification agent	20-80 vol% H_2O/N_2
Flow rate (mL/min, S.T.P), reduction	800
Purge	100% N_2
Oxidation agent	100% air
Flow rate (mL/min, S.T.P), oxidation	800

Table 4 Effect of steam content on the reaction performance, 900^{o}C, δ=1.77

Variables	**Parameters**					
H_2O%	**$r_{volat,inst}$**	**$\eta_{c,volat}$**	**$m_{FR,volat}$**	**$r_{char,inst}$**	**$\eta_{c,char}$**	**$m_{FR,char}$**
(vol%)	**(%/min)**	**(-)**	**(kg/MW_{th})**	**(%/min)**	**(-)**	**(kg/MW_{th})**
20	84	0.62	535	84	0.92	840
40	84	0.63	545	204	0.94	350
80	-	-	-	204	0.96	350

Table 5 Effects of oxygen potential oxygen ratio δ and temperature on the char combustion, steam content 80 vol%

Variables		**Parameters**	
Temperature	$\boldsymbol{\delta}$	$\boldsymbol{r_{char,inst}}$	$\boldsymbol{\eta_{c,\ char}}$
(^{o}C)	**(-)**	**(%/min)**	**(-)**
900	1.77	204	0.96
950	1.77	204	0.97
1000	1.77	288	0.97
1000	1.18	-	0.91
1000	0.88	-	0.86